

Advancing potential field data analysis: the Modified Horizontal Gradient Amplitude method (MHGA)

Hanbing AI¹ , Hazel DENIZ TOKTAY² , Ahmad ALVANDI^{3,*} , Roman PAŠTEKA⁴ , Kejia SU⁵ , Qiang LIU⁶

¹ School of Geophysics and Geomatics, China University of Geosciences, Wuhan 430074, China; e-mail: hanbingai@foxmail.com

² Department of Geophysical Engineering, Istanbul University – Cerrahpaşa, Istanbul, Turkey; e-mail: hazel.deniztoktay@iuc.edu.tr

³ Institute of Geophysics, University of Tehran, Tehran, Iran; e-mail: aalvandi@ut.ac.ir

⁴ Department of Engineering Geology, Hydrogeology and Applied Geophysics, Faculty of Sciences, Comenius University, Ilkovičova 6, 842 15 Bratislava, Slovak Republic; e-mail: roman.pasteka@uniba.sk

⁵ Research Institute No.270, CNNC, Nanchang, Jiangxi, 330200, China; e-mail: sukejia2022@163.com

⁶ China Aero Geophysical Survey and Remote Sensing Center for Natural Resources, Beijing 100083, China; e-mail: 1191881251@qq.com

Abstract: Enhancing the detection accuracy of the edges of the geological features within the subsurface remains a significant objective in geophysical data interpretation. Despite numerous advancements, approaches stemming from the directional gradients of gravity and magnetic fields still grapple with challenges such as low-resolution outcomes and susceptibility to noise contamination. In this study, we introduce a novel filtering framework based on the total horizontal gradient and its derivatives, designed to yield more precise and coherent edges free from false boundaries or disruptive artifacts. Validation using synthetic Bishop complex magnetic and gravity datasets, alongside Tuangiao aeromagnetic data from Vietnam, substantiates the robustness and applicability of our modified approach. Furthermore, recognizing the inherent susceptibility of edge detection filters to noise contamination resulting from directional derivatives, we employ the recently developed modified non-local means (MNLM) algorithm to alleviate noise effects prior to the analysis of noisy synthetic and real datasets. Our findings confirm the efficacy of the proposed method in reducing false artifacts and identifying edges with heightened precision, positioning MHGA as a valuable alternative for processing potential field data.

Key words: edge detection, modified non-local means, horizontal gradient amplitude, aeromagnetic data

*corresponding author, e-mail: aalvandi@ut.ac.ir

1. Introduction

Magnetic and gravity field measurements made on the ground, in the air, and via satellites provide crucial details about the subsurface geological structures (Narayan et al., 2021). Magnetic and gravity field methods are less expensive and have broad applications compared to some geophysical methods (Ekinçi et al., 2023; Ai et al., 2023a; Toktay et al., 2021). Edge detectors are constantly used to map subsurface geologic structures through gravity and magnetic data interpretation (Fedi and Florio, 2001; Ekinçi et al., 2013; Sun et al., 2016; Chen et al., 2017; Nasuti and Nasuti, 2018; Weihermann et al., 2018; Pham et al., 2019; Pham et al., 2021; Prasad et al., 2022; Alvandi and Ardestani, 2023; Alvandi et al., 2023a; Ibraheem et al., 2023). Numerous distinct methodologies have been devised for the extraction of buried source boundaries, primarily relying on directional differentials of potential field anomalies (Alvandi et al., 2023a). Cordell and Grauch (1985) employed the total horizontal gradient or horizontal gradient amplitude method (HGA) to delineate the horizontal boundaries. The HGA approach of reduced-to-pole (RTP) magnetic field or gravity field can be expressed as:

$$\text{HGA} = \sqrt{\left(\frac{\partial P}{\partial x}\right)^2 + \left(\frac{\partial P}{\partial y}\right)^2}. \quad (1)$$

In equation (1), $\frac{\partial P}{\partial x}$ and $\frac{\partial P}{\partial y}$ are the first-order horizontal derivatives of potential field data. Roest et al. (1992) used the maximum values of the analytic signal amplitude or total gradient (ASA) filter to indicate the buried source edges. The ASA expressed as follows:

$$\text{ASA} = \sqrt{\left(\frac{\partial P}{\partial x}\right)^2 + \left(\frac{\partial P}{\partial y}\right)^2 + \left(\frac{\partial P}{\partial z}\right)^2}. \quad (2)$$

In relation (2), the first-order vertical derivative of potential field data is given as $\frac{\partial P}{\partial z}$. However, HGA and ASA filters perform unsatisfactorily in highlighting the buried source edges (Saibi et al., 2012; Prasad et al., 2022; Alvandi and Ardestani, 2023). Numerous normalized filters have been proposed, incorporating the ratio or combination of directional derivatives derived from potential field data, aimed at simultaneously capturing all

boundaries of shallow-level and deep-seated buried sources. The popular tilt angle or tilt derivative (TA) method is the first normalized method introduced by *Miller and Singh (1994)*. In TA, the vertical gradient of the field is normalized by its HGA. The TA relationship is given by:

$$\text{TA} = \tan^{-1} \left(\frac{\frac{\partial P}{\partial z}}{\sqrt{\left(\frac{\partial P}{\partial x}\right)^2 + \left(\frac{\partial P}{\partial y}\right)^2}} \right). \quad (3)$$

Verduzco et al. (2004) showed that the use of the maximum amplitude of the HGA of the TA (HGATA) can provide the horizontal boundaries more precisely. The HGATA is expressed as:

$$\text{HGATA} = \sqrt{\left(\frac{\partial \text{TA}}{\partial x}\right)^2 + \left(\frac{\partial \text{TA}}{\partial y}\right)^2}. \quad (4)$$

Cooper and Cowan (2006) proposed a detector (TDX) using the normalized horizontal gradient amplitude of the field P. This method yields maxima indicative of subsurface structural edges and it is given by:

$$\text{TDX} = \tan^{-1} \left(\frac{\sqrt{\left(\frac{\partial P}{\partial x}\right)^2 + \left(\frac{\partial P}{\partial y}\right)^2}}{\left| \frac{\partial P}{\partial z} \right|} \right). \quad (5)$$

In efforts to enhance the efficacy of horizontal gradient amplitude for detecting the boundaries of causative sources, *Ferreira et al. (2013)* introduced the tilt angle of the total horizontal gradient (TAHGA), which is calculated as follows:

$$\text{TAHGA} = \tan^{-1} \left(\frac{\frac{\partial \text{HGA}}{\partial z}}{\sqrt{\left(\frac{\partial \text{HGA}}{\partial x}\right)^2 + \left(\frac{\partial \text{HGA}}{\partial y}\right)^2}} \right). \quad (6)$$

The improved horizontal tilt angle (ITDX), or normalization of the vertical gradient's HGA by the modulus of the second-order vertical gradients

(SVD), was first introduced by *Ma et al. (2016)*. The method is defined as:

$$\text{ITDX} = \tan^{-1} \left(\frac{\sqrt{\left(\frac{\partial^2 P}{\partial z \partial x}\right)^2 + \left(\frac{\partial^2 P}{\partial z \partial y}\right)^2}}{\left|\frac{\partial^2 P}{\partial z^2}\right|} \right). \tag{7}$$

An additional normalized method introduced by *Nasuti et al. (2019)*, referred to as the HGA of the STDR, serves as a potent processing tool for accentuating buried source boundaries. The technique is calculated as:

$$\text{HGASTD} = \sqrt{\left(\frac{\partial \text{STDR}}{\partial x}\right)^2 + \left(\frac{\partial \text{STDR}}{\partial y}\right)^2}, \tag{8}$$

where

$$\text{STDR} = \tan^{-1} \left(\frac{W \times \frac{\partial^2 P}{\partial z^2}}{\sqrt{\left(\frac{\partial \text{HGA}}{\partial x}\right)^2 + \left(\frac{\partial \text{HGA}}{\partial y}\right)^2}} \right). \tag{9}$$

In the relation (9), W represents a positively selected numerical value by the interpreter. Here, we applied $W = 900.000$ for gravity data and $W = 50.000$ for RTP magnetic data, as recommended by *Nasuti et al. (2019)*. Although the normalized techniques (TA, HGATA, TDX, TAHGA, ITDX and HGASTD) can map both the deep-seated and shallow-situated causative sources, they tend to produce spurious and ambiguous lateral boundaries when dealing with some cases (*Ghomsi et al., 2022; Pham et al., 2022; Alvandi and Ardestani, 2023*). This study endeavors to formulate a pioneering normalized methodology originating from HGA directional derivatives for the precise delineation of horizontal boundaries within subsurface structures, aiming for heightened resolution and minimized false edge occurrences. We effectively showcased the utilization of the proposed methodology on synthetic responses (generated by prisms and the Bishop model) under varying noise conditions, as well as on a real-world dataset obtained from the Tuangiao region of Vietnam.

2. Proposed new edge detector with modified non-local means filter

2.1. Modified horizontal gradient amplitude (MHGA)

The arctangent and hyperbolic tangent functions have been applied to most of the detectors introduced in gravity and magnetic data edge detection filters (*Ibraheem et al., 2023*). Nevertheless, it should be noted that the hyperbolic tangent function possesses a narrower range compared to the arctangent function (*Ibraheem et al., 2023*). The created filter is inspired by the linear saturated function, which is similar to the hyperbolic tangent function. We have introduced this technique with the aim of augmenting the resolution and precision of delineated lateral boundaries by refining the total horizontal gradient method. The proposed modified horizontal gradient amplitude (MHGA) technique uses an enhanced form of the ratio of the first-order vertical and horizontal gradients of the horizontal gradient amplitude of the gravity and RTP magnetic data, expressed as:

$$\text{MHGA} = \frac{|\text{R} + 1| - |\text{R} - 1|}{2}, \quad (10)$$

where

$$\text{R} = \left(\frac{\frac{\partial \text{HGA}}{\partial z}}{\sqrt{\left(\frac{\partial \text{HGA}}{\partial x}\right)^2 + \left(\frac{\partial \text{HGA}}{\partial y}\right)^2}} - \frac{\pi}{3} \right). \quad (11)$$

We emphasize that the vertical derivative $\frac{\partial \text{HGA}}{\partial z}$ in the numerator is not the true vertical derivative, but so-called k-function (*Florio et al., 2006*) or pseudo-vertical derivative (*de Souza et al., 2024*), as it is computed within the spectral domain using the conventional approach of vertical derivative assessment (*Pham et al., 2019; Pham and Oliveira, 2023*). This property does not influence the good recognition properties of the MHGA transform. The amplitude of the MHGA is between -1 and 1 , and the amplitude maxima are located at the edges of the causative sources. The main advantage of the MHGA is that it exhibits horizontal boundaries with great precision and sharpness. The resolution of the adjusted horizontal gradient amplitude result is unaffected by parameters chosen by the interpreter, in contrast to

contemporary high-resolution methods. (Pham et al., 2019; Nasuti et al., 2019; Alvandi and Ardestani, 2023; Alvandi et al., 2023b). Given that MHGA is derived from the ratio of derivatives pertaining to the total horizontal gradient, it facilitates a clearer mapping of the edges of deep sources when contrasted with the total horizontal gradient approach.

2.2. Modified non-local means filter

The Modified Non-Local Means (MNLM) filter, introduced by Ai et al. (2023b), represents a recent advancement in noise attenuation algorithms. This filter integrates unweighted Euclidean distance with Integral Image techniques to mitigate the uncertainty and complexity associated with tuning control parameters, while also expediting the weight calculation process inherent to the traditional Non-Local Means (NLM) method. Extensive testing by Ai et al. (2023b) has demonstrated the efficacy of MNLM in denoising potential field data by optimizing three algorithmic control parameters Ds , ds , and h . The intrinsic reason of the high performance of MNLM lies in the weight selection process, it retains the advantage of NLM, concerning a wide range of information instead of information limited within a local neighbourhood, but obtains the weights in a simpler and faster way. Consequently, MNLM is particularly effective for mitigating noise effects exacerbated by high-order gradient calculation-based edge detectors, such as MHGA. For comprehensive mathematical details and implementation procedures of the MNLM filter, refer to Ai et al. (2023b).

3. The synthetic example

3.1. 2D model

In order to substantiate the efficacy of the proposed filter, we constructed a 2D synthetic magnetic model. The model comprises three vertical prisms buried at different depths with distinct properties. The parameters associated with the causative sources are shown in Fig. 1. The magnetic response of the synthetic data in Fig. 1a and its reduced-to-pole (RTP) magnetic data are shown in Fig. 1b. The response of different conventional and normalized procedures (HGA, ASA, TA, HGATA, TDX, TAHGA, ITDX, HGASTD, and MHGA) is shown in Figs. 1c to 1k. The results of edge enhancement

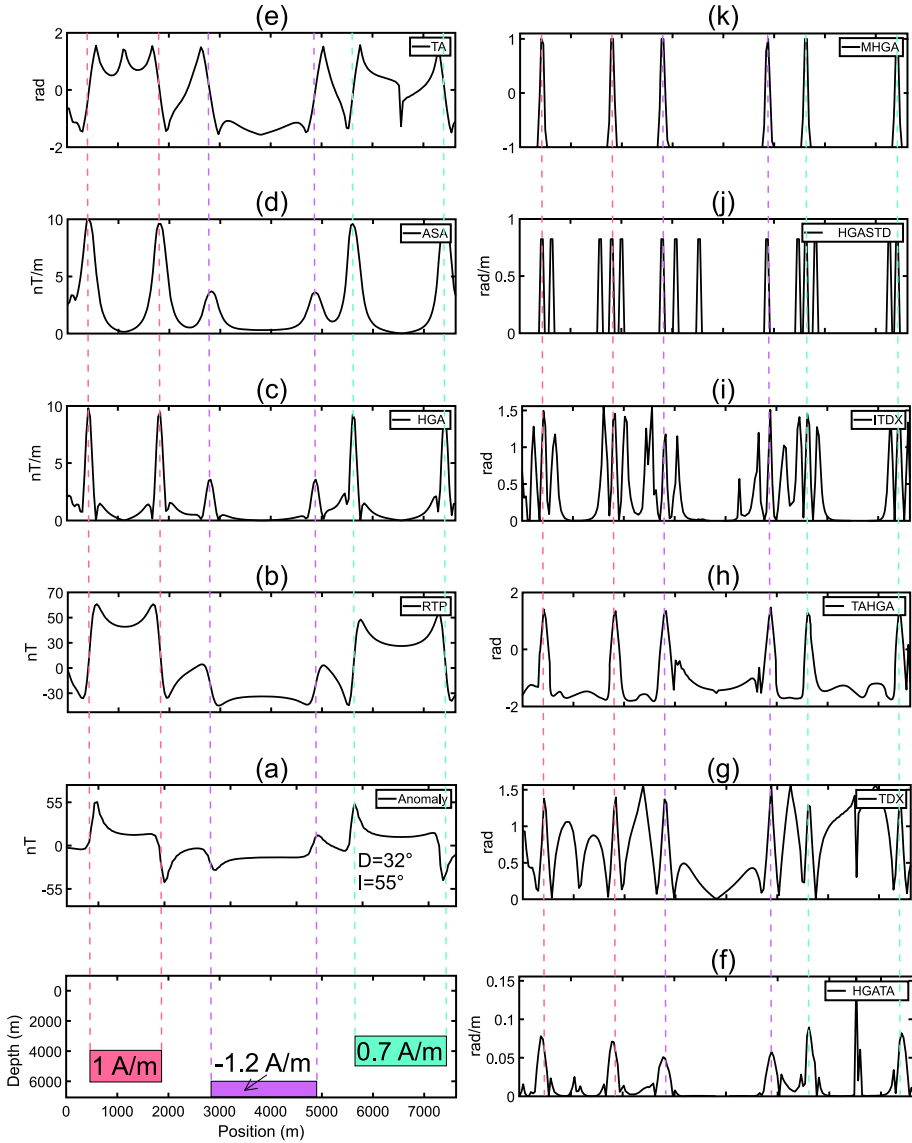


Fig. 1. The response of different edge detection techniques over a magnetic dike-like model and an illustrative depiction of the synthetic model: (a) the response of the magnetic anomaly to the three prismatic bodies; (b) the RTP magnetic anomaly. The responses of the different filters are shown as (c) HGA, (d) ASA, (e) TA, (f) HGATA, (g) TDX, (h) TAHGA, (i) ITDX, (j) HGASTD, and (k) MHGA.

demonstrate that the analysis of responses in the HGA and ASA methods is notably improved when magnetic data are subjected to various normalized and standard filters. However, the response must be balanced for the shallow and deeper bodies. The TA, HGATA, TDX, ITDX, and HGASTD filters produce spurious and false boundaries, making interpretation much more difficult. Both the TAHGA and MHGA methods excel in accurately mapping all edges without any occurrence of false information. However, the peaks of MHGA show a clearer and more balanced delineation of the horizontal boundaries of the dike-like bodies (Fig. 1k).

In the subsequent sections, the efficacy of the proposed detector is evaluated through a comparative analysis of its 3D outputs against those generated by alternative methods including HGA, ASA, TA, HGATA, TDX, TAHGA, ITDX, and HGASTD.

3.2. 3D prismatic model

The integrity of the presented new method is further assessed using synthetic 2D magnetic datasets under the presence and absence of noise. The first 3D example is comprised of six prisms. Fig. 2 illustrates both the perspective and planar views of the synthetic 3D magnetic model. The properties of the causative bodies are presented in Table 1. The magnetic anomalies associated with these bodies were computed at 6000×6000 observation points, employing a 100-meter sampling interval through the algorithm of *Rao and Babu (1991)* (Fig. 2c).

Table 1. Geometric parameters and geomagnetic susceptibility values of the synthetic 3D geomagnetic model.

Parameters/Label	M1	M2	M3	M4	M5	M6
X coordinate of the Centre (m)	2000	2000	4000	2300	1400	1900
Y coordinate of the Centre (m)	4000	4000	4000	2000	1400	1800
The width of Prism (m)	2000	1200	45	50	30	20
The length of Prism (m)	2000	500	10000	10000	10000	10000
Depth to the Top (m)	200	200	100	70	55	50
Depth to the Bottom (m)	300	215	600	570	555	550
Azimuth of Strike (°)	45	35	5	55	95	120
Susceptibility of magnetized body (SI)	0.010	0.025	0.030	0.025	0.020	0.010

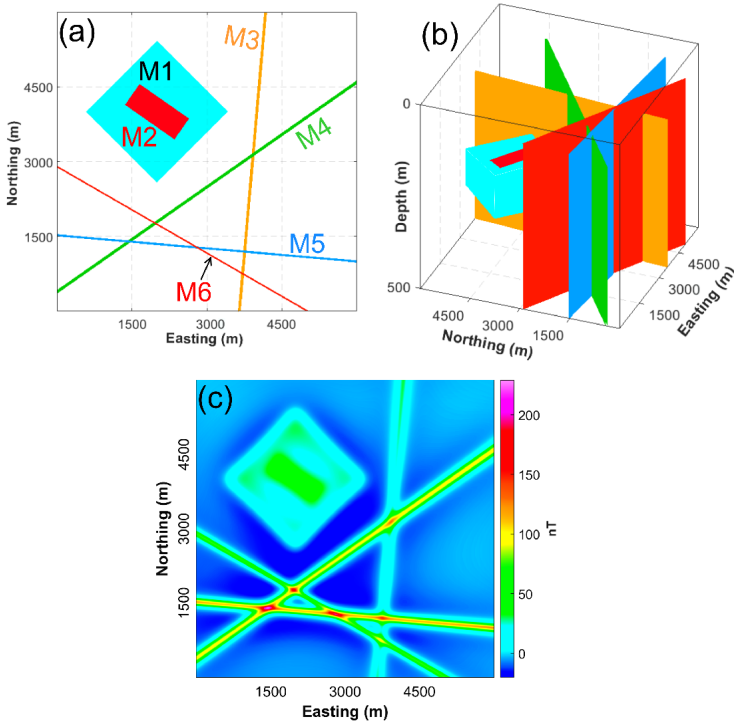


Fig. 2. The 3D synthetic magnetic model: a) 3D view, b) planar view, and c) magnetic anomaly of the model.

Figures 3a and b present the lateral boundaries extracted by applying the HGA and ASA techniques to the anomaly in Fig. 2c, respectively. It is evident from these figures that the large amplitude response of the shallow sources M4, M5, and M6 dominates the HGA and ASA maps, while the edges of the deeper sources M1 and M2 are discernibly attenuated. Figure 3c presents the TA of the magnetic anomaly in Fig. 2c. The TA anomaly prominently amplifies anomalies attributed to the bodies M1, M3, M4, M5, and M6, albeit inducing some spurious edges surrounding the source M2. Figure 3d exhibits the HGATA result of a geomagnetic anomaly in Fig. 2c. The HGATA technique exhibits a lack of distinct gradient across horizontal boundaries, resulting in attenuated delineation of the edges associated with both deep and shallow sources M1, M2, M3, M4, M5, and M6. Figure 3e presents the demarcated borders achieved through the utilization of

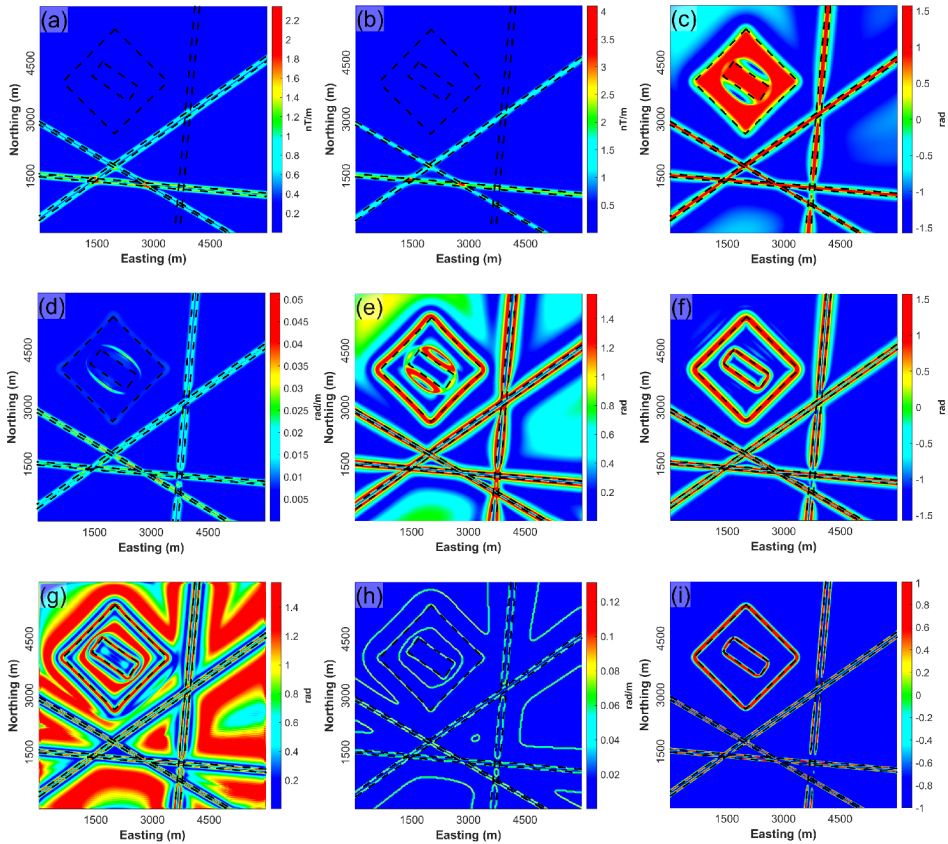


Fig. 3. Edge detection maps of data shown in Fig. 2c. a) HGA, b) ASA, c) TA, d) HGATA, e) TDX, f) TAHGA, g) ITDX, h) HGASTD, i) MHGA. Dashed lines represent the actual borders.

the TDX filter on the magnetic dataset depicted in Fig. 2c. While the TDX technique successfully delineates the lateral boundaries of both shallow and deep anomalies, it introduces spurious edges around source M2, resulting in diffuse edge estimations. Figure 3f exhibits the boundaries obtained by the TAHGA technique. The detector exhibits the capability to concurrently delineate edges situated at both shallow and deep depths. Despite the effectiveness of TAHGA in mapping all edges, the resultant edge image demonstrates a reduction in resolution. Figure 3g presents the edges estimated by applying the ITDX filter to magnetic data in Fig. 2c. As depicted in this

figure, the ITDX outlines the edges at different depths but creates several false edges between and around the buried anomalies. Figure 3h depicts the edges obtained by the HGASTD detector. Although the HGASTD exhibits sharp edges for the sources, it also brings spurious edges between or around the sources M1, M2, M3, M4, M5, and M6. Figure 3i presents the edges detected by the proposed MHGA approach. Like the ITDX and HGASTD methods, MHGA demonstrates the capacity to offer edges at a heightened resolution in comparison to HGA, ASA, TA, HGATA, TDX, and TAHGA filters. Nonetheless, the proposed approach is distinguished by its ability to delineate all source edges without artificial boundaries, in contrast to ITDX and HGASTD.

Figure 4a depicts the magnetic anomaly from Figure 2c, augmented with Gaussian-type noise with standard deviation of 5 nT, facilitating a synthetic investigation into the noise effect. The noise influence increases inherently because the detectors are based on horizontal and vertical gradients. To attenuate the noise contamination, we applied a modified non-local means (MNLM) filter (*Ai et al., 2023b*) before applying the different detectors aforementioned and the MHGA filter proposed (Fig. 4b). The MNLM algorithm is an effective filter proposed recently for denoising potential field data (*Ai et al., 2023b*). As depicted in Fig. 4b, the application of the MNLM filter yields a more homogeneous representation, while retaining the fundamental shapes of the synthetic magnetic model. The control parameters of

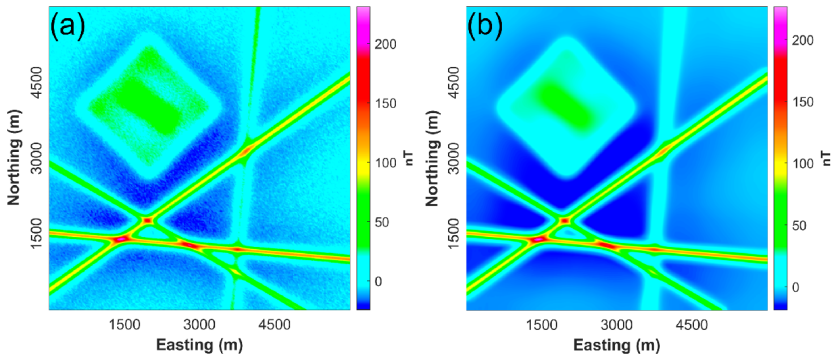


Fig. 4. a) noisy magnetic anomaly from the synthetic response in Fig. 2c; b) filtered result using the modified non-local means algorithm (the parameters of MNLM are $ds = 3$, $Ds = 15$, $h = 0.07 * \min(\max(\text{noisy data}))$).

MNLM are $ds = 3$, $Ds = 15$, $h = 0.07 * \min(\max(\sim))$. $\min(\sim)$ and $\max(\sim)$ are two functions returning the minimum elements of an array and maximum elements of a column of numbers, respectively.

Figures 5a and b display the edges obtained from the HGA and ASA detectors, respectively. The large signals again dominated both filters and responded from the shallow bodies M4, M5, and M6. The boundaries of the deep sources M1, M2, and M3 are so faintly observed. Figure 5c displays anomalies calculated from the TA filter. In this case, the TA effectively enhances five buried sources but fails to detect the edges of the source

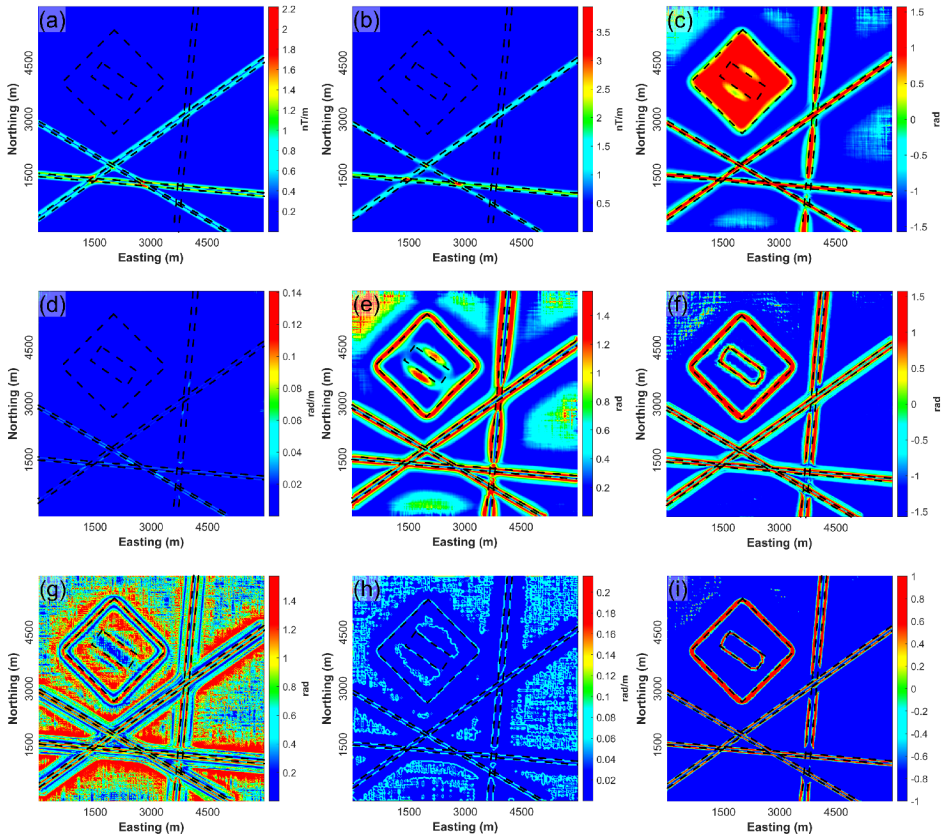


Fig. 5. Edge detection maps of the data shown in Fig. 4b. a) HGA, b) ASA, c) TA, d) HGATA, e) TDX, f) TAHGA, g) ITDX, h) HGASTD, i) MHGA. Dashed lines represent the actual borders.

M2. Once more, HGATA exhibits a deficiency in concurrently enhancing edges originating from both deep and shallow sources, resulting in faint delineations (Fig. 5d). Figure 5e depicts the response calculated from the TDX approach. In this instance, the TDX approach effectively enhances five buried sources, yet falls short in delineating the edges of buried source M2. Figure 5f illustrates the boundaries delineated by the TAHGA detector. This method effectively generates an equalized image for body edges. However, the edges in the TAHGA map exhibit diffusion. Figures 5g and 5h present the boundaries calculated from the ITDX and HGASTD filters, respectively. As depicted in these images, the ITDX and HGASTD filters are more susceptible to noise compared to other detectors. This susceptibility arises from their reliance on the second vertical derivative (SVD) of the data. Additionally, the ITDX and HGASTD filters generate spurious boundaries around the structures. Figure 5i displays the boundaries delineated by the proposed detector, MHGA. Notably, the MHGA filter, in conjunction with the MNLM denoising method, prominently depicts all edges in the presence of random noise. The MHGA method exhibits fewer noise features compared to the ITDX and HGASTD methods, and it does not produce spurious boundaries around or above bodies M1, M2, M3, M4, M5, and M6. Furthermore, the MHGA still yields high-resolution edge maps in this case.

3.3. The Bishop complex model

This section employs the proposed technique to Bishop's complex synthetic gravity (BCSG) data to assess its effectiveness (*Williams et al., 2005; Alvandi and Ardestani, 2023*). Several authors have applied the BCSG data for edge enhancement (*Cooper, 2020; Dwivedi and Chamoli, 2021; Chen and Zhang, 2022; Alvandi and Ardestani, 2023; Al-Bahadily et al., 2024*). Figure 6 displays the basement depth and gravity anomaly of BCSG. The BCSG model portrays minor faults along with two comparatively extensive, large-offset faults, delineated by the black dashed lines in Fig. 6a (*Florio, 2018*). The unfaulted deep basin region is situated in the southeast corner, while shallow structures are positioned northwest of the BCSG depiction (Fig. 6b). In this study, the BCSG model with and without Gaussian noise were considered to evaluate the effectiveness of the MHGA detector.

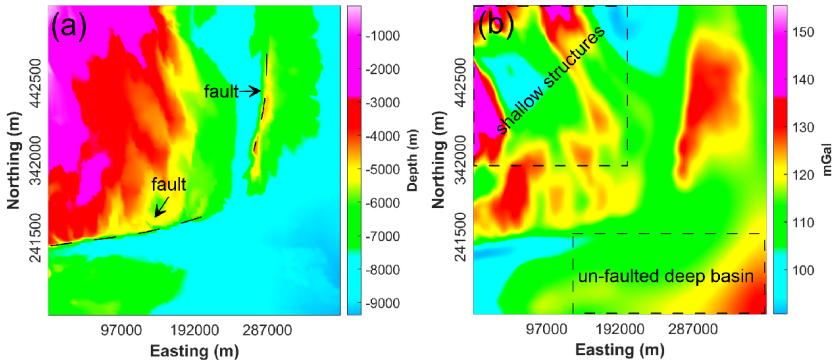


Fig. 6. a) Basement depth of the Bishop synthetic model (the dashed lines illustrate major faults) (*Williams et al., 2005*); b) Gravity anomaly of the BCSG (the closed dashed lines indicate the locations of shallow and deep buried sources).

Figures 7a–i show the processed results of the various detectors dealing with the noise-free BCSG data. As depicted in Figs, 7a-b, the outcomes of the HGA and ASA methodologies are predominantly influenced by shallow-level sources, respectively, resulting in the blurring of the two primary faults. The HGA and ASA filters cannot depict the unfaulted deep basin sources. Figures 7c and d show the TA and HGATA of the data in Fig. 6b, respectively. In this case, the TA is effective in enhancing shallow buried sources but fails to detect edges of the deep sources (the unfaulted deep basin region), and again, the HGATA fails to enhance any edges from the deep and shallow sources simultaneously. Lateral boundaries are faint, and the edges detected are ambiguous. Figure 6e presents the edges extracted from the TDX method. This method is effective in creating edges for shallow sources. In this experiment, it is observed that all five filters (HGA, ASA, TA, HGATA, and TDX) exhibit limitations in effectively detecting the edges of deep or thin structures. Figure 6f presents the edges extracted from the TAHGA detector. This method effectively generates an equalized image for the buried source edges. However, the lateral boundaries in the TAHGA map are diffuse. In this instance, the ITDX approach fails to accurately identify the edges of the structures situated in the southeast corner of the edge detection map, thereby resulting in the generation of spurious edges in the output image (Fig. 7g). The HGASTD and MHGA filters can equal-

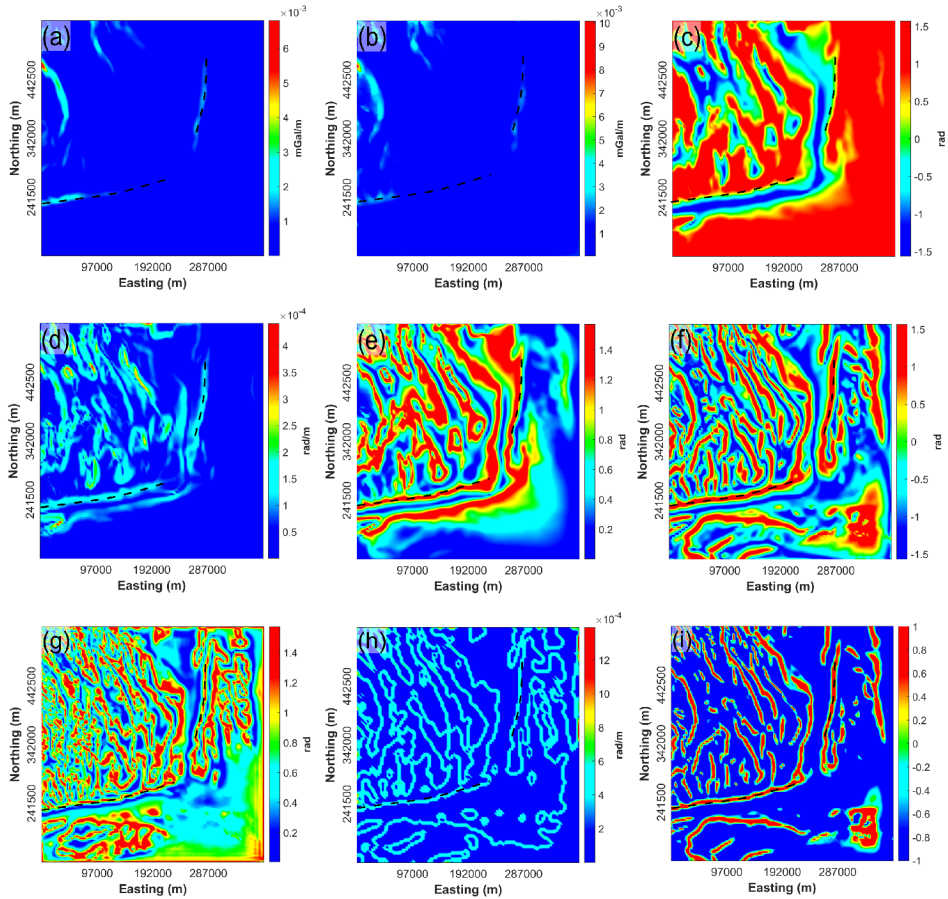


Fig. 7. Edge detection maps of the data shown in Fig. 6b. a) HGA, b) ASA, c) TA, d) HGATA, e) TDX, f) TAHGA, g) ITDX, h) HGASTD, i) MHGA. Dashed lines represent the location of faults.

ize the edges of buried bodies with different depths and other properties. However, the HGASTD detector generates false borders around and above the buried structures (Fig. 7h). The MHGA filter offers superior resolution in comparison to alternative filters. It effectively reconciles the anomalies originating from both shallow and deep-level sources, while successfully delineating edges associated with both primary and minor structures (Fig. 7i).

In the context of the BCSG illustration, the robustness of the proposed method and other detectors against random noise was evaluated by delin-

eating the edges of the gravity model while accounting for the noise presence in the observed anomaly (Fig. 8a). This noise, characterized as Gaussian, possesses an amplitude corresponding with standard deviation of 3 mGal depicted in Fig. 6b. To attenuate the added Gaussian noise, we applied the modified non-local means algorithm again before applying the different detectors and proposed approach (Fig. 8b). The parameters of MNLM are $ds = 3$, $Ds = 18$, $h = 0.3 * \min(\max(\text{noisy gravity data}))$.

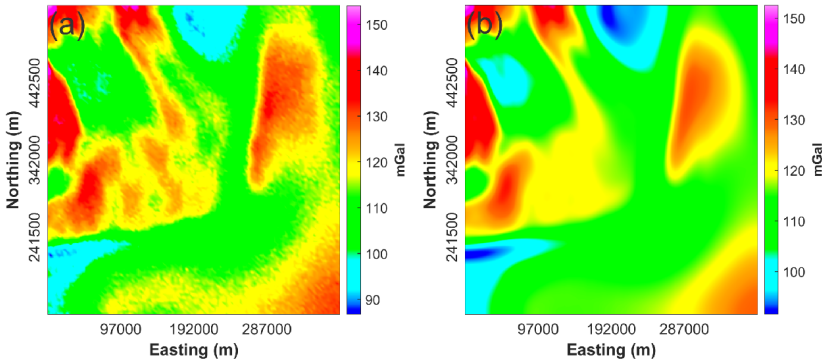


Fig. 8. a) Noisy gravity anomaly from the BCSG model in Fig. 6b; b) filtered anomaly using the modified non-local means algorithm (the parameters of MNLM are $ds = 3$, $Ds = 18$, $h = 0.3 * \min(\max(\text{noisy gravity data}))$).

Figures 9a and b depict the lateral boundaries extracted from the HGA and ASA filters, respectively. Once again, both methodologies are predominantly influenced by the pronounced signals originating from shallow-level sources. Figures 9c and 9d illustrate anomalies derived from the TA and HGATA methodologies, respectively. Since the HGATA filter is derived from derivatives of the TA, it tends to be more susceptible to noise compared to the TA alone. While the TA method can effectively map shallow buried sources, in this instance, the HGATA is overwhelmed by the strong signals emanating from the shallower bodies, resulting in faint and indistinct edges. Figures 9e and 9f present the lateral boundaries extracted using the TDX and TAHGA techniques, respectively. The TAHGA approach successfully generates well-balanced images of the source edges, while the TDX method fails to enhance any edges from the deep, unfaulted basin region. However, the lateral boundaries delineated in the TAHGA maps appear

diffuse. Figures 9g and 9h depict the boundaries derived from the ITDX and HGASTD methods, respectively. These images reveal that the ITDX and HGASTD filters are more susceptible to noise compared to other filters, as they are based on the second vertical derivative (SVD) of the data. Figure 9i displays the lateral boundaries detected by the MHGA method, yielding the boundary information with high resolution and without false edges.

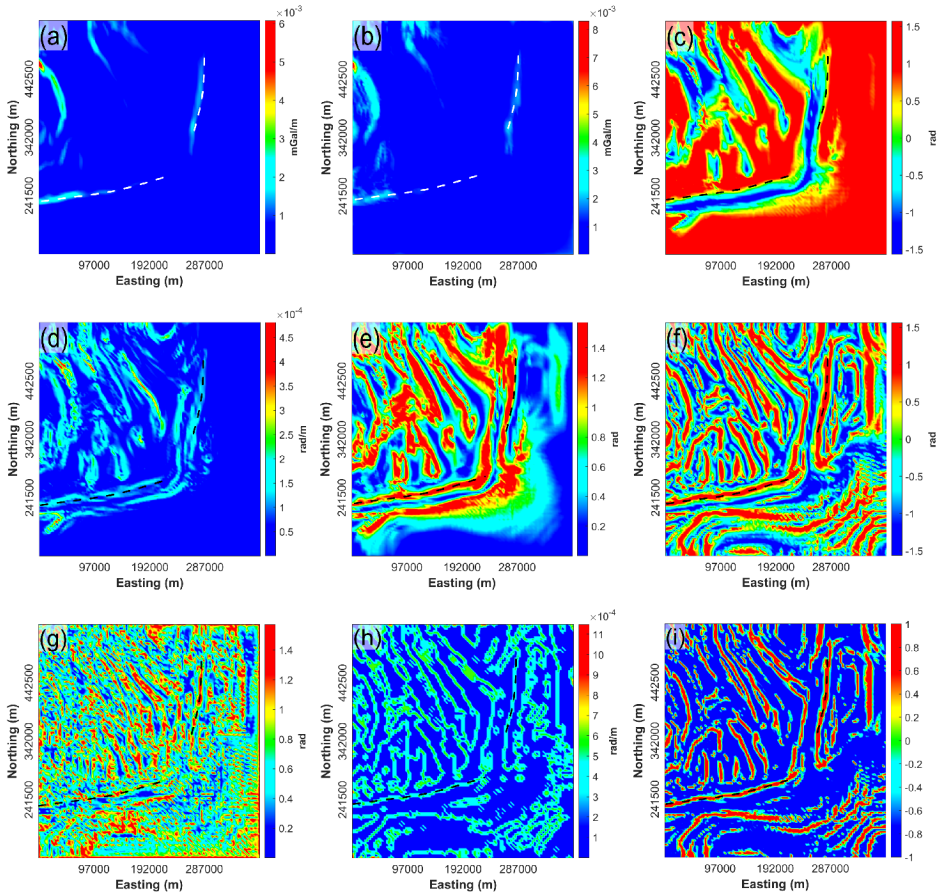


Fig. 9. Edge detection maps of data in Fig. 8b: a) HGA, b) ASA, c) TA, d) HGATA, e) TDX, f) TAHGA, g) ITDX, h) HGASTD, i) MHGA. Dashed lines indicate the location of faults.

4. Real example

The validity of the presented new method is examined using aeromagnetic anomaly data from Tuangiao, Vietnam (Fig. 10). Figure 10 illustrates the geological map of the region and its surroundings (Koszowska et al., 2007). The Tuangiao region comprises seven principal structural units oriented in a southeast-northwest direction, namely the Fan SiPan massif, Tu Le basin, Song Da rift, Song Ma zone, Sam Nua-An Chau terrane, Truong Son Fold Belt, and Sibumasu terrane (Koszowska et al., 2007; Hieu et al., 2012; Pham, 2023). Seismic activity in this area is primarily associated with faults trending southeast-northwest (Pham et al., 2021; Pham, 2023). The aeromagnetic data from Tuangiao were acquired in 1998 by the Geophysical Division of Vietnam (Fig. 11a). RTP aeromagnetic data calculated using inclination = 31° and declination = -0.7° is shown in Fig. 11b. Denoised RTP aeromagnetic data using the modified non-local means algorithm is shown in Fig. 11c. The parameters of MNLM are $ds = 7$, $Ds = 15$, $h = 0.01 * \min(\max(\text{the real data}))$.

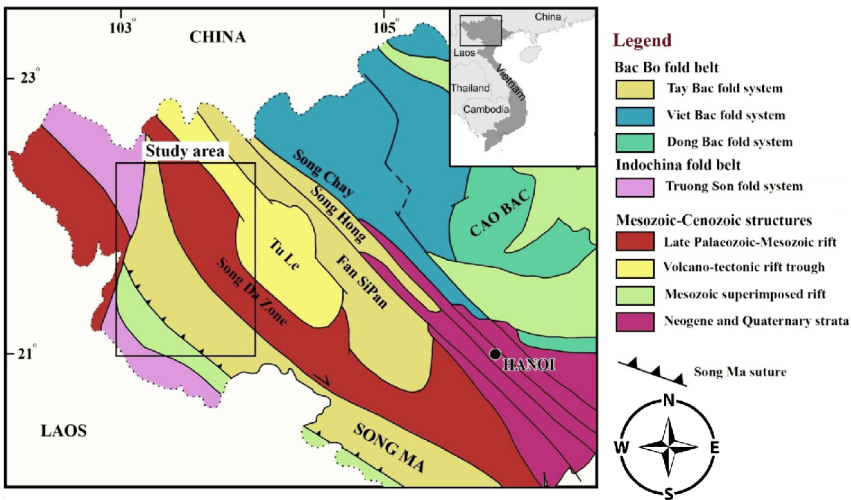


Fig. 10. The geological map of the Tuangiao area and its surroundings (Koszowska et al., 2007; Pham 2023).

Figure 12a displays the HGA map of the RTP aeromagnetic data for Tuangiao. As illustrated in this image, the HGA method is primarily in-

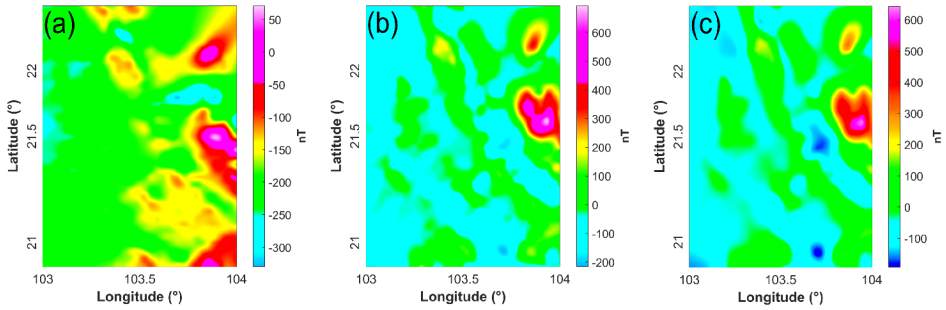


Fig. 11. a) Aeromagnetic data; b) RTP aeromagnetic anomaly; c) Denoised RTP aeromagnetic data of the Tuangiao area (the parameters of MNLM are $ds = 7$, $Ds = 15$, $h = 0.01 * \min(\max(\text{the real data}))$).

fluenced by significant amplitude anomalies, consequently rendering it incapable of providing a dependable output for the structural configuration of the studied area. Figure 12b presents the ASA map derived from the RTP aeromagnetic data. It is evident that the ASA map is predominantly affected by large amplitude anomalies, thereby failing to generate an accurate depiction of the buried sources within the study area. Figure 12c displays the result of the TA. One can see that the edges extracted by this filter are diffused. Figure 12d displays the lateral boundary image calculated using the HGATA. The method fails to achieve an equalized representation of magnetic causative sources, with the buried structures extracted from HGATA exhibiting significant faintness. Figure 12e presents the structure edges extracted by the TDX. In this case, the TDX detector generates spurious edges. Figure 12f presents the borders generated from the TAHGA approach. This method effectively creates an equalized image for the buried source edges of the area studied. However, the lateral boundaries depicted in the TAHGA map exhibit diffusion. Figures 12g and h depict the lateral boundaries the ITDX and HGASTD estimated, respectively. Although both filters are capable of generating structural images with relatively high resolution, they result in intricate edge maps. The 2D and 3D theoretical examples show that these filters bring spurious borders around and above the buried structures. Figure 12i depicts the edges detected by the MHGA. Similar to normalized detectors, the MHGA effectively normalizes anomalies of varying amplitudes. Furthermore, the MHGA is capable of generating product-structured images with high resolution. As demonstrated in the

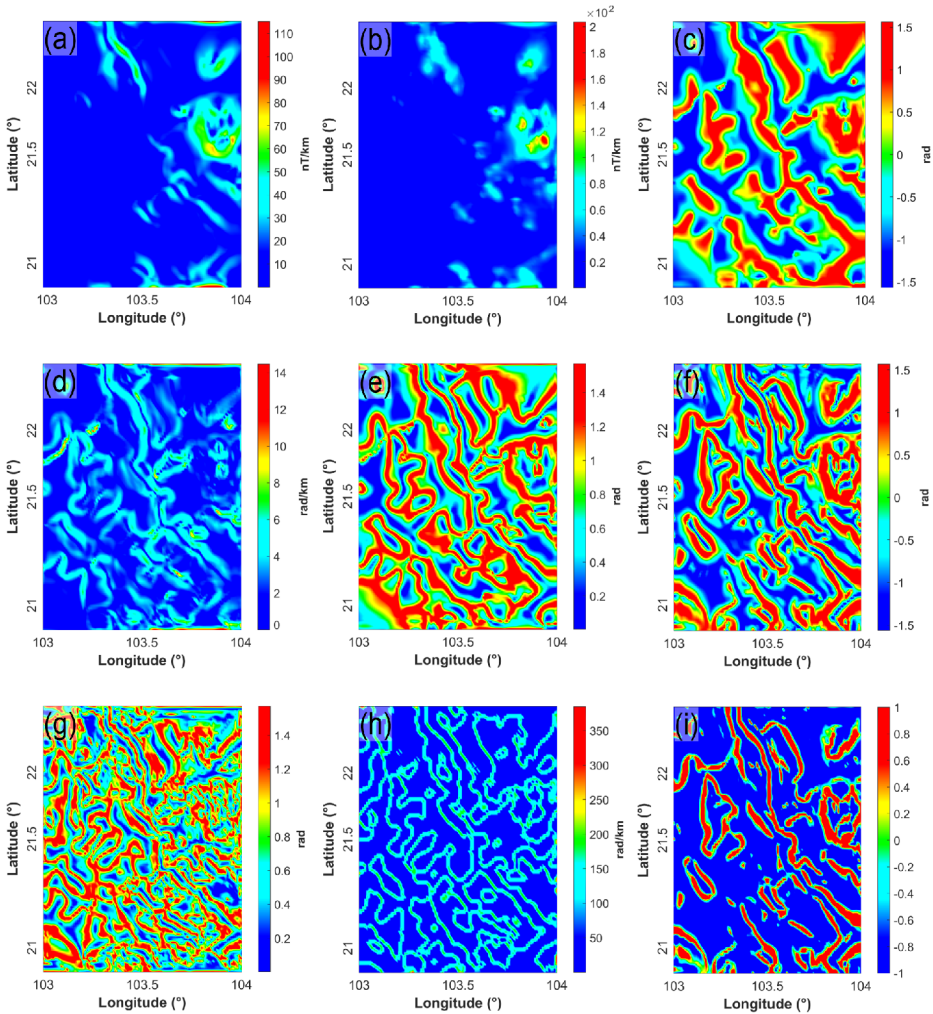


Fig. 12. Edge detection maps of data shown in Fig. 11c. a) HGA, b) ASA, c) TA, d) HGATA, e) TDX, f) TAHGA, g) ITDX, h) HGASTD, i) MHGA.

MHGA map (Fig. 12i), the introduced filter facilitated the extraction of a diverse array of structures within the Tuangiao area. A comparison between the proposed filter and the geological map (Fig. 10) reveals that the boundaries delineated by the MHGA detector exhibit a strong correlation

with the southeast-northwest trending structures prevalent in the Tuangiao region.

In addition to detecting lateral boundaries, the depth determination of causative structures is also valuable for interpreting aeromagnetic data (Alvandi *et al.*, 2022). In this work, we employed the tilt-depth method to estimate the depth of the buried sources retrieved (Salem *et al.*, 2008). Figure 13a depicts the result of applying the tilt-depth method to the study region. The rose diagram and histogram illustrating the calculated depths are presented in Figs. 13b and 13c, indicating that 50% of the structures are situated at depths ranging from 2 to 4 km. The predominant top depth of the majority of edges varies between 1 and 12 km, exhibiting random disturbances across the Tuangiao region. In Figure 13a, the edges are overlaid on the tilt-depth map to facilitate detailed comparisons. The locations of the buried source points demonstrate a significant correlation with the edges extracted by the MHGA approach. Furthermore, numerous edges align with geological features. Thus, through the integration of the processed results from MHGA and the tilt-depth filter, both qualitative and quantitative interpretations of the Tuangiao region can be conducted reliably.

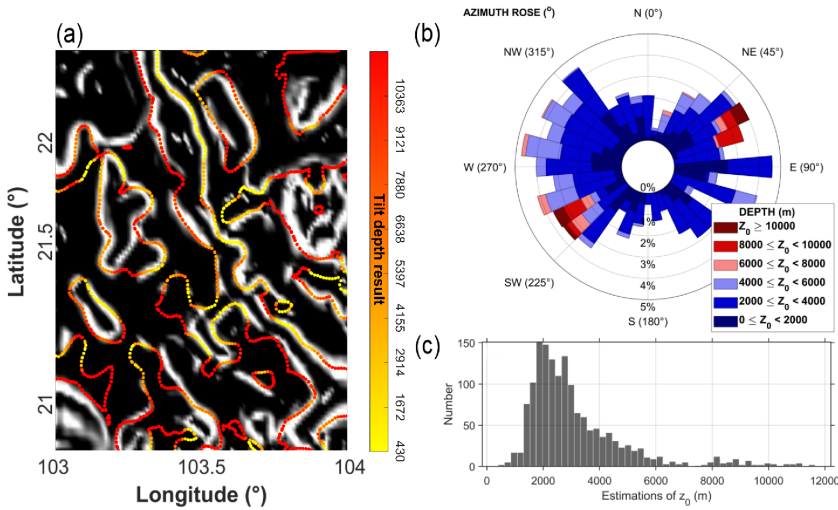


Fig. 13. a) The depths calculated from the tilt-depth method (retrieved geological edges from Fig. 12i) are superimposed on the tilt-depth method result); (b) The rose diagram derived from the tilt-depth method; (c) The histogram of the top depth calculated from the tilt-depth method.

5. Conclusions

A modified version of the HGA detector (MHGA), namely the modified horizontal gradient amplitude, has been introduced to enhance the causative source edges from potential field data more precisely. The proposed methodology has been validated utilizing synthetic gravity data generated from the Bishop model, magnetic data simulated from an imposed prismatic model, and real-world aeromagnetic data obtained from the Tuangiao region of Vietnam. Comparative analysis reveals that the MHGA approach excels in delineating the lateral boundaries present within gravity and magnetic datasets with enhanced precision and resolution. Furthermore, it effectively mitigates the occurrence of spurious edges while simultaneously highlighting shallow and deep structures.

Funding. Not applicable.

Author contributions. All authors have contributed to the conceptualization of this research and the computational implementation of the methods. H. A. and A. A. collaborated on the mathematical framework, conducted the data selection, and prepared the manuscript. H. D. T. and R. P. contributed to the revision process. K. S. and Q. L. controlled the figures. All authors have thoroughly reviewed and consented to the final version of the manuscript for publication.

Data availability statement. The data pertaining to the Bishop basement model, along with their corresponding descriptions, can be accessed at https://wiki.seg.org/wiki/Bishop_Model. Related computer codes of the filter, MNLM, can be accessed at the GitHub platform (<https://github.com/HanbingAi/Gravity-anomaly-denoising-using-Modified-Non-Local-Means>).

Acknowledgements. The authors extend their thanks to Dr. Luan Thanh Pham for his guidance in collecting the aeromagnetic data in the Tuangiao area of Vietnam.

References

- Ai H., Ekinçi Y. L., Balkaya Ç., Essa K. S., 2023a: Inversion of geomagnetic anomalies caused by ore masses using hunger games search algorithm. *Earth Space Sci.*, **10**, 11, e2023EA003002, doi: 10.1029/2023EA003002.
- Ai H., Alvandi A., Ghanati R., Pham L. T., Alarifi S. S., Nasui D., Eldosouky A. M., 2023b: Modified non-local means: A novel denoising approach to process gravity field data. *Open Geosci.*, **15**, 1, 20220551, doi: 10.1515/geo-2022-0551.

- Al-Bahadily H. A., Al-Rahim A. M., Smith R. S., 2024: Determination of reactivated regions and faults in the Iraq Southern Desert with the new edge technique, Inverse Tilt Angle of Second-gradients (ITAS). *Acta Geophys.*, **72**, 3, 1675–1692, doi: 10.1007/s11600-023-01176-4.
- Alvandi A., Toktay H. D., Nasri S., 2022: Application of direct source parameter imaging (direct local wave number) technique to the 2-D gravity anomalies for depth determination of some geological structures, for depth determination of some geological structures. *Acta Geophys.*, **70**, 2, 659–667, doi: 10.1007/s11600-022-00750-6.
- Alvandi A., Ardestani V. E., 2023: Edge detection of potential field anomalies using the Gompertz function as a high-resolution edge enhancement filter. *Bull. Geophys. Oceanogr.*, **64**, 3, 279–300, doi: 10.4430/bgo00420.
- Alvandi A., Su K., Ai H., Ardestani V. E., Lyu C., 2023a: Enhancement of Potential Field Source Boundaries Using the Hyperbolic Domain (Gudermannian Function). *Minerals*, **13**, 10, 1312, doi: 10.3390/min13101312.
- Alvandi A., Toktay H., Ardestani V. E. Z., 2023b: Edge detection of geological structures based on a logistic function: a case study for gravity data of the Western Carpathians. *Int. J. Min. Geo-Eng.*, **57**, 3, 267–274, doi: 10.22059/IJMGE.2023.353516.595018.
- Chen A.-G., Zhou T.-F., Liu D.-J., Zhang S., 2017: Application of an enhanced theta-based filter for potential field edge detection: A case study of the luzong ore district. *Chin. J. Geophys.*, **60**, 2, 203–218, doi: 10.1002/cjg2.30039.
- Chen T., Zhang G., 2022: NHF as an edge detector of potential field data and its application in the Yili Basin. *Minerals*, **12**, 2, 149, doi: 10.3390/min12020149.
- Cooper G. R. J., Cowan D. R., 2006: Enhancing potential field data using filters based on the local phase. *Comput. Geosci.*, **32**, 10, 1585–1591, doi: 10.1016/j.cageo.2006.02.016.
- Cooper G. R. J., 2020: A modified enhanced horizontal derivative filter for potential field data. *Explor. Geophys.*, **51**, 5, 549–554, doi: 10.1080/08123985.2020.1725386.
- Cordell L., Grauch V. J. S., 1985: Mapping Basement Magnetization Zones from Aeromagnetic Data in the San Juan Basin. In: Hinze W. J. (Ed.): *The Utility of Regional Gravity and Magnetic Anomaly Maps*. SEG Publication, New Mexico, 181–197, doi: 10.1190/1.0931830346.ch16.
- Dwivedi D., Chamoli A., 2021: Source edge detection of potential field data using wavelet decomposition. *Pure Appl. Geophys.*, **178**, 3, 919–938, doi: 10.1007/s00024-021-02675-5.
- de Souza J., Oliveira S. P., Szameitat L. S. A., de Souza Filho O. A., Ferreira F. J. F., 2024: Fourier domain vertical derivative of the non-potential squared analytical signal of dike and step magnetic anomalies: A case of serendipity. *Geophysics*, **89**, 2, G1–G12, doi: 10.1190/geo2022-0760.1.
- Ekinçi Y. L., Ertekin C., Yiğitbaş E., 2013: On the effectiveness of directional derivative based filters on gravity anomalies for source edge approximation: synthetic simulations and a case study from the Aegean graben system (western Anatolia, Turkey). *J. Geophys. Eng.*, **10**, 3, 035005, doi: 10.1088/1742-2132/10/3/035005.

- Ekinci Y. L., Balkaya Ç., Göktürkler G., Ai H., 2023: 3-D gravity inversion for the basement relief reconstruction through modified success-history-based adaptive differential evolution. *Geophys. J. Int.*, **235**, 1, 377–400, doi: 10.1093/gji/ggad222.
- Fedi M., Florio G., 2001: Detection of potential fields source boundaries by enhanced horizontal derivative method. *Geophys. Prospect.*, **49**, 1, 40–58, doi: 10.1046/j.1365-2478.2001.00235.x.
- Ferreira F. J. F., de Souza J., Bongiolo A. B. S., Castro L. G., 2013: Enhancement of the total horizontal gradient of magnetic anomalies using the tilt angle. *Geophysics*, **78**, 3, J33–J41, doi: 10.1190/geo2011-0441.1.
- Florio G., 2018: Mapping the depth to basement by iterative rescaling of gravity or magnetic data. *J. Geophys. Res. Solid Earth*, **123**, 10, 9101–9120, doi: 10.1029/2018JB015667.
- Florio G., Fedi M., Pašteka R., 2006: On the application of Euler deconvolution to the analytic signal. *Geophysics*, **71**, L87–L93, doi: 10.1190/1.2360204.
- Ghomsi F. E. K., Pham L. T., Tenzer R., Esteban F. D., Vu T. V., Kamguia J., 2022: Mapping of fracture zones and structural lineaments of the Gulf of Guinea passive margins using marine gravity data from CryoSat-2 and Jason-1 satellites. *Geocarto Int.*, **37**, 25, 10819–10842, doi: 10.1080/10106049.2022.2040602.
- Hieu P. T., Chen F., Me L. T., Thuy N. T. B., Siebel W., Lan T.-G., 2012: Zircon U-Pb ages and Hf isotopic compositions from the Sin Quyen Formation: the Precambrian crustal evolution of northwest Vietnam. *Int. Geol. Rev.*, **54**, 13, 1548–1561, doi: 10.1080/00206814.2011.646831.
- Ibraheem I. M., Tezkan B., Ghazala H., Othman A. A., 2023: A new edge enhancement filter for the interpretation of magnetic field data. *Pure Appl. Geophys.*, **180**, 6, 2223–2240, doi: 10.1007/s00024-023-03249-3.
- Koszowska E., Wolska A., Zuchiewicz W., Cuong N. Q., Pécskay Z., 2007: Crustal contamination of Late Neogene basalts in the Dien Bien Phu Basin, NW Vietnam: Some insights from petrological and geochronological studies. *J. Asian Earth Sci.*, **29**, 1, 1–17, doi: 10.1016/j.jseaes.2005.12.003.
- Ma G., Huang D., Liu C., 2016: Step-edge detection filters for the interpretation of potential field data. *Pure Appl. Geophys.*, **173**, 3, 795–803, doi: 10.1007/s00024-015-1053-6.
- Miller H. G., Singh V., 1994: Potential field tilt—a new concept for location of potential field sources. *J. Appl. Geophys.*, **32**, 2-3, 213–217, doi: 10.1016/0926-9851(94)90022-1.
- Narayan S., Kumar U., Pal S. K., Sahoo S. D., 2021: New insights into the structural and tectonic settings of the Bay of Bengal using high-resolution earth gravity model data. *Acta Geophys.*, **69**, 6, 2011–2033, doi: 10.1007/s11600-021-00657-8.
- Nasuti Y., Nasuti A., 2018: NTilt as an improved enhanced tilt derivative filter for edge detection of potential field anomalies. *Geophys. J. Int.*, **214**, 1, 36–45, doi: 10.1093/gji/ggy117.
- Nasuti Y., Nasuti A., Moghadas D., 2019: STDR: a novel approach for enhancing and edge detection of potential field data. *Pure Appl. Geophys.*, **176**, 2, 827–841, doi: 10.1007/s00024-018-2016-5.

- Pham L. T., 2023: A novel approach for enhancing potential fields: application to aeromagnetic data of the Tuangiao, Vietnam. *Eur. Phys. J. Plus*, **138**, 12, 1134, doi: 10.1140/epjp/s13360-023-04760-1.
- Pham L. T., Kafadar O., Oksum E., Eldosouky A. M., 2021: An improved approach for detecting the locations of the maxima in interpreting potential field data. *Arab. J. Geosci.*, **14**, 1, 43, doi: 10.1007/s12517-020-06399-z.
- Pham L. T., Oksum E., Do T. D., Le-Huy M., Vu M. D., Nguyen V. D., 2019: LAS: A combination of the analytic signal amplitude and the generalized logistic function as a novel edge enhancement of magnetic data. *Contrib. Geophys. Geod.*, **49**, 4, 425–440, doi: 10.2478/congeo-2019-0022.
- Pham L. T., Oksum E., Kafadar O., Trong T. P., Nguyen V. D., Vo Q. T., Le S. T., Do T. D., 2022: Determination of subsurface lineaments in the Hoang Sa islands using enhanced methods of gravity total horizontal gradient. *Vietnam J. Earth Sci.*, **44**, 3, 395–409, doi: 10.15625/2615-9783/17013.
- Pham L. T., Oliveira S. P., 2023: Edge enhancement of magnetic sources using the tilt angle and derivatives of directional analytic signals. *Pure Appl. Geophys.*, **180**, 12, 4175–4189, doi: 10.1007/s00024-023-03375-y.
- Prasad K. N. D., Pham L. T., Singh A. P., 2022: Structural mapping of potential field sources using BHG filter. *Geocarto Int.*, **37**, 26, 11253–11280, doi: 10.1080/10106049.2022.2048903.
- Rao D. B., Babu N. R., 1991: A rapid method for three-dimensional modeling of magnetic anomalies. *Geophysics*, **56**, 11, 1729–1737, doi: 10.1190/1.1442985.
- Roest W. R., Verhoef J., Pilkington M., 1992: Magnetic interpretation using the 3-D analytic signal. *Geophysics*, **57**, 1, 116–125, doi: 10.1190/1.1443174.
- Saibi H., Aboud E., Ehara S., 2012: Analysis and Interpretation of gravity data from the Aluto-Langano geothermal field of Ethiopia. *Acta Geophysica*, **60**, 2, 318–336, doi: 10.2478/s11600-011-0061-x.
- Salem A., Williams S., Fairhead D., Smith R., Ravat D., 2008: Interpretation of magnetic data using tilt-angle derivatives. *Geophysics*, **73**, 1, L1–L10, doi: 10.1190/1.2799992.
- Sun Y., Yang W., Zeng X., Zhang Z., 2016: Edge enhancement of potential field data using spectral moments. *Geophysics*, **81**, 1, G1–G11, doi: 10.1190/geo2014-0430.1.
- Toktay H. D., Aydoğan D., Yüksel F. A., 2021: Quantitative analysis of total magnetic anomaly maps on archaeological sites—Part 1. *Math. Methods Appl. Sci.*, **44**, 17, 13696–13710, doi: 10.1002/mma.7652.
- Verduzco B., Fairhead J. D., Green C. M., Mackenzie C., 2004: New insights into magnetic derivatives for structural mapping. *Lead. Edge*, **23**, 2, 116–119, doi: 10.1190/1.1651454.
- Weihermann J. D., Ferreira F. J. F., Oliveira S. P., Cury L. F., de Souza J., 2018: Magnetic interpretation of the Paranaguá Terrane, southern Brazil by signum transform. *J. Appl. Geophys.*, **154**, 116–127, doi: 10.1016/j.jappgeo.2018.05.001.
- Williams S. E., Fairhead J. D., Flanagan G., 2005: Comparison of grid Euler deconvolution with and without 2D constraints using a realistic 3D magnetic basement model. *Geophysics*, **70**, 3, L13–L21, doi: 10.1190/1.1925745.